UC Berkeley
UC Berkeley Previously Published Works

Title
Voltage-sensitive rhodol with enhanced two-photon brightness.

Permalink
https://escholarship.org/uc/item/74z3q8q1

Journal
Proceedings of the National Academy of Sciences of the United States of America, 114(11)

ISSN
0027-8424

Authors
Kulkarni, Rishikesh U
Kramer, Daniel J
Pourmandi, Narges
et al.

Publication Date
2017-03-01

DOI
10.1073/pnas.1610791114

Peer reviewed

Voltage-sensitive rhodol with enhanced two-photon brightness

Rishikesh U. Kulkarni[a,1], Daniel J. Kramer[b,1], Narges Pourmandi[a], Kaveh Karbasi[a], Helen S. Bateup[b,c], and Evan W. Miller[a,b,c,2]

[a]Department of Chemistry, University of California, Berkeley, CA 94720; [b]Department of Molecular and Cell Biology, University of California, Berkeley, CA 94720; and [c]Helen Wills Neuroscience Institute, University of California, Berkeley, CA 94720

We have designed, synthesized, and applied a rhodol-based chromophore to a molecular wire-based platform for voltage sensing to achieve fast, sensitive, and bright voltage sensing using two-photon (2P) illumination. Rhodol VoltageFluor-5 (RVF5) is a voltage-sensitive dye with improved 2P cross-section for use in thick tissue or brain samples. RVF5 features a dichlororhodol core with pyrrolidyl substitution at the nitrogen center. In mammalian cells under one-photon (1P) illumination, RVF5 demonstrates high voltage sensitivity (28% ΔF/F per 100 mV) and improved photostability relative to first-generation voltage sensors. This photostability enables multisite optical recordings from neurons lacking tuberous sclerosis complex 1, Tsc1, in a mouse model of genetic epilepsy. Using RVF5, we show that Tsc1 KO neurons exhibit increased activity relative to wild-type neurons and additionally show that the proportion of active neurons in the network increases with the loss of Tsc1. The high photostability and voltage sensitivity of RVF5 is recapitulated under 2P illumination. Finally, the ability to chemically tune the 2P absorption profile through the use of rhodol scaffolds affords the unique opportunity to image neuronal voltage changes in acutely prepared mouse brain slices using 2P illumination. Stimulation of the mouse hippocampus evoked spiking activity that was readily discerned with bath-applied RVF5, demonstrating the utility of RVF5 and molecular wire-based voltage sensors with 2P-optimized fluorophores for imaging voltage in intact brain tissue.

voltage imaging | fluorescent sensors | two-photon microscopy

Neurons communicate by translating electrical signals (membrane potential) into chemical signals (neurotransmitter release). Neuronal membrane potential dynamics drive neurotransmitter release and are therefore responsible for the unique physiology associated with neurons at cellular, circuit, and organismal levels. Despite the central importance of proper neuronal firing to human health, an integrated understanding of neuronal activity in the context of larger brain circuits remains elusive, due in part to a lack of methods for interrogating membrane potential dynamics with sufficient spatial and temporal resolution.

Traditional methods for monitoring membrane potential rely heavily on the use of invasive electrodes, through one of two methods. The first method, patch-clamp electrophysiology, uses a single electrode to make contact with or puncture a cell to record changes in membrane potential, sacrificing throughput and spatial resolution to achieve a comprehensive description of a single cellular electrophysiological profile. A second method uses multielectrode arrays (MEAs), in which patterned arrays of electrodes introduced to cells or tissues report on electrical changes. Spatial resolution of MEAs depends on the number and positioning of the electrodes within the array. Although throughput is improved relative to patch-clamp electrophysiology, the extracellularly recorded signals are typically less sensitive than whole-cell methods and can be an amalgamation of several cells, making deconvolution of recorded signals and precise correlation to specific cells difficult or impossible. Additionally, it is impossible

to tell if a "silent" MEA channel is a result of poor electrode positioning or because the neuron itself is silent (1).

Direct imaging of voltage changes with fluorescent probes is an attractive solution to these challenges because voltage imaging can provide the spatial and temporal resolution needed to match signals to cells with high throughput and fidelity (2, 3). The challenge of achieving optical voltage sensing is a long-standing goal within the scientific community (4, 5), and recent approaches have included fluorinated styryl dyes (6), annulated hemicyanines (7, 8) and cyanines (9), lipophilic anions (10, 11), hybrid small-molecule/fluorescent protein probes (12, 13), porphyrins (14), and nanoparticles (15, 16). However, combinations of poor sensitivity, slow kinetics, ineffective membrane localization, rapid photobleaching, and/or limited two-photon cross-section, which is important for imaging in thick tissue, have hampered rapid progress toward a general solution for optical voltage imaging. Small-molecule voltage sensors in particular are plagued by trade-offs in speed and sensitivity. More recently, genetically encoded fluorescent voltage sensors also show promise in terms of both speed and sensitivity (17–20), but current methods are similarly limited by low one- and two-photon brightness (21).

We were therefore drawn to a method for voltage sensing that makes use of a photoinduced electron transfer (PeT) (22) through a molecular wire as a voltage-sensitive trigger (23). PeT-based molecular wire voltage sensors, or VoltageFluors (VF), intercalate into the plasma membrane so that the direction of PeT aligns perpendicular to the plane of the plasma membrane

Significance

Fast changes in membrane potential drive the unique physiology of neurons. Despite the critical importance of coordinated neuronal firing, observing neuronal activity in a noninvasive, highly parallel manner remains an outstanding challenge, due in part to a lack of tools that can report on fast changes in membrane potential with sufficient speed, sensitivity, and brightness. We report an optical voltage reporter based on a fluorescent rhodol that shows improved photostability and brightness under both one- and two-photon illumination. We use the indicator RhodolVoltageFluor-5 to probe dynamics of neuronal excitability in a mouse model of genetic epilepsy, both in culture and in brain slices.

Fig. 1. Voltage sensing via PeT using 1P or 2P excitation and synthesis of RVF5. (*A*) At hyperpolarized or resting potentials (*Left*), fluorescence is quenched via PeT, whereas at depolarized potentials (*Right*), PeT is inhibited by the electric field across the membrane, enhancing fluorescence. Voltage sensitivity can be achieved under traditional 1P illumination with blue light (1P, cyan arrow) or with two photons of infrared light (2P, dark-red arrow). (*B*) Synthesis of RVF5.

(Fig. 1) (24). PeT within a VF dye is enhanced under hyperpolarized cellular conditions (negative intracellular charge) and decreased during cellular depolarization (positive intracellular charge). Because the rate of PeT competes with the rate of fluorescence, cellular hyperpolarization, corresponding to typical resting neuronal membrane potential, results in a dim fluorescent state from the VF dye, whereas depolarization gives fluorescence enhancement, enabling the detection of fast-spiking action potentials in neurons.

Small-molecule fluorescent voltage sensors based on a PeT trigger show promise for interrogating membrane potential dynamics in neuronal systems because these VF, or VF dyes, display good sensitivity, excellent response times, and avoid complications associated with added capacitance. Additionally, because VF dyes are small molecules, they should be readily tunable to a number of different chromophores (25) to select for desired properties, such as wavelength (26), improved photostability, or enhanced two-photon cross-section (27). In this article, we describe the design, synthesis, characterization, and application of Rhodol VoltageFluor-5 (RVF5), a voltage-sensitive small molecule in the VoltageFluor family with enhanced photostability and improved two-photon optical cross-section relative to the parent fluorescein-based VF dyes. We use RVF5 to show that molecular wire-based voltage sensors can operate under two-photon illumination and to probe neuronal excitability in a mouse model of the human genetic epilepsy disorder Tuberous Sclerosis Complex (TSC), both in cultured neurons and in acutely prepared brain slices.

Results and Discussion

Design and Synthesis of RVF5. We reasoned that the conversion of fluorescein-based VF dyes into unsymmetrical rhodol-based reporters, in which one of the oxygen atoms at the 3'- and 6' positions of the xanthene chromophore is replaced by a substituted nitrogen (28), would improve photostability and two-photon absorbance (σ_2). Introduction of asymmetry in the chromophore axis increases the extent of intramolecular charge transfer, enhancing efficiency of σ_2 (measured in Göppert–Mayer units of 10^{-50} cm^4 s photon^{-1}·molecule^{-1}) (27). Furthermore, rhodols exhibit higher photostabilty than their oxygen-substituted xanthene counterparts (29). Both properties—improved photostability and σ_2—would significantly improve our ability to monitor changes in neuronal voltage for extended periods of time and in thick, optically opaque tissues. RVF5 is available in two steps from a first-generation VF dye (Fig. 1). Triflation of the original VF dye, VF2.1.Cl, **1** with triflic anhydride and triethylamine in dimethylformamide provided intermediate **2** in 70% yield, following silica gel chromatography. Subsequent nucleophilic aromatic substitution (S$_N$Ar) with pyrrolidine at 90 °C

provided RVF5 in 27% yield, following purification by reversed-phase semipreparative HPLC.

Spectroscopic and Cellular Characterization of RVF5. RVF5 displays excitation and emission profiles centered in the visible range, with a λ_{max} of 520 nm ($\varepsilon_{520} = 83{,}000$ cm^{-1}·M^{-1}, PBS, pH 7.4) and a secondary absorbance at 395 nm ($\varepsilon_{395} = 45{,}000$ cm^{-1}·M^{-1}) corresponding to the phenylenevinylene molecular wire (*SI Appendix*, Fig. S1) RVF5 emits at 535 nm ($\Phi_{fl} = 0.27$, PBS, pH 7.4; *SI Appendix*, Fig. S1). Bath application of RVF5 to HEK cells at 37 °C for 15 min results in clear fluorescence intensity associated with the membrane (Fig. 2*A*). External membrane localization was confirmed upon near-complete loss of membrane-associated fluorescence when RVF5-loaded cells were treated with buffer containing FBS (FBS, 1%; *SI Appendix*, Fig. S2). To assess the photostability of RVF5 under cellular illumination conditions, we loaded HEK cells with either RVF5 or VF2.1.Cl and monitored membrane-associated fluorescence over time (475 nm, 2.3 W/cm^2). Under typical illumination conditions RVF5 exhibits approximately fivefold greater photostability compared with VF2.1.Cl (Fig. 2*B* and *SI Appendix*, Fig. S3), with a decay constant of 5.6×10^{-4}·s^{-1} for RVF5 and 2.8×10^{-3}·s^{-1} for VF2.1.Cl.

To confirm that membrane-associated RVF5 fluorescence in HEK cells is voltage sensitive, HEK cells were stained with RVF5 (200 nM) and subjected to whole-cell patch-clamp electrophysiology under voltage clamp conditions. Cells were held at a membrane potential of −60 mV to simulate resting potential for a typical mammalian neuron and then hyper- and depolarized to various potentials ranging from −100 mV to +100 mV in 20-mV increments (Fig. 2*C*). As predicted, and as demonstrated
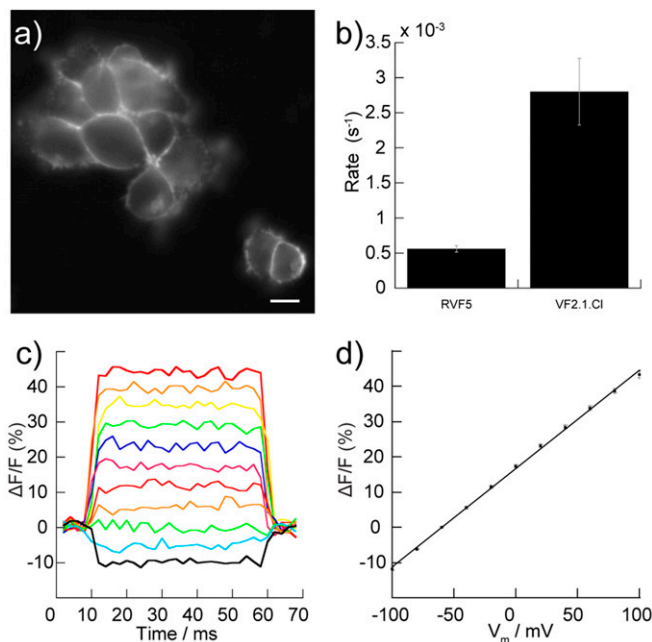
Fig. 2. One photon, epifluorescence characterization of RVF5 in HEK cells. (*A*) Wide-field fluorescence image of HEK cells stained with 200 nM RVF5 for 15 min at 37 °C. (*B*) Relative photostability of RVF5 compared with VF2.1.Cl. Error bars are ±SEM for $n = 5$ experiments. Voltage sensitivity of RVF5 in HEK cells was assayed by patch-clamp electrophysiology. (*C*) Fractional change in RVF5 fluorescence (ΔF/F) vs. time in an HEK cell held under voltage clamp at −60 mV and then subjected to potentials ranging from +100 mV to −100 mV for 50 ms in 20-mV increments. Concatenated traces shown in *C* are representative of a single experiment. (*D*) Fractional change in fluorescence (ΔF/F) vs. final membrane potential (V$_m$), in millivolts. Error bars are ±SEM for $n = 7$ experiments. (Scale bar, 10 μm.)
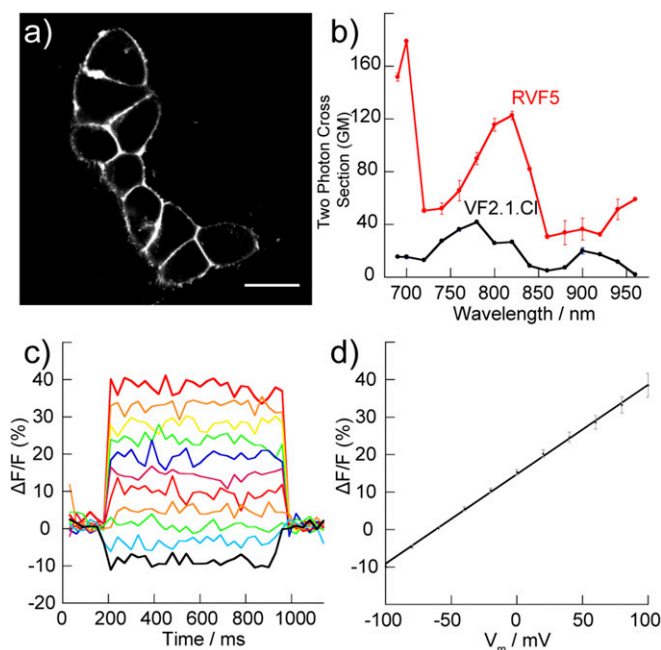
Fig. 3. Two-photon characterization of RVF5 in HEK cells. (*A*) Two-photon scanning laser microscopy image of HEK cells stained with 1 μM RVF5 for 15 min at 37 °C. (*B*) Comparison of 2P cross-section of RVF5 (red) and VF2.1.Cl (black) vs. wavelength in vitro (PBS, pH 7.4). Error bars are ±SEM for $n = 3$ experiments. (*C*) Fractional change in fluorescence (ΔF/F) vs. time in a patch-clamped HEK cells under 2P illumination (820 nm), held at –60 mV and then stepped to potentials ranging from –100 to +100 mV in 20-mV increments. Traces shown are for a single cell. (*D*) ΔF/F vs. final membrane potential (V_m) in millivolts. Error bars are ±SEM for $n = 3$ experiments. (Scale bar, 10 μm.)

for previous classes of PeT-based voltage sensors (23, 24, 26), depolarization results in fluorescence enhancement from the cell membrane whereas hyperpolarization decreases membrane fluorescence (Fig. 2*C*). Plotting fractional change in fluorescence (ΔF/F) vs. potential gives a linear voltage sensitivity of 28% (±1%) ΔF/F per 100 mV over a range spanning ±100 mV, comparable to the voltage sensitivity of the first generation of xanthene-based VF dyes (27% ΔF/F per 100 mV) (Fig. 2*D*).

Two-Photon Optical Properties of RVF5. We next sought to determine the two-photon optical properties of RVF5. Two-photon absorption relies on the essentially instantaneous delivery of two low-energy photons to promote a chromophore from the ground state to the excited state (27), and is beneficial for imaging in thick tissue because lower-energy photons scatter less, cause less tissue damage, and, in the case of two-photon microscopy, reduce out-of-plane illumination because of the quadratic dependence of two-photon absorbance on incident light intensity (30). We measured the two-photon absorption cross-section (σ_{TPA}) of RVF5 and VF2.1.Cl in solution by normalizing to a rhodamine B standard (*SI Appendix*) (31–33). A plot of two-photon cross-section vs. excitation wavelength reveals a σ_{TPA} maximum of 120 GM at 820 nm for RVF5 (Fig. 3*B*), which corresponds well to literature values for a related rhodol (115 GM at 820 nm, in ethanol) (34). For comparison, VF2.1.Cl displays a weaker σ_{TPA}, ~40 GM at its λ_{max} of 780 nm.

Other voltage-sensitive fluorophores like the widely used ANEPPS family display maximum two-photon absorbance values in the range of 5–10 GM (35); eGFP has maximum two-photon absorbance value of 30–40 GM at 925 nm (30). The two-photon absorbance value for VF2.1.Cl at 820 nm is 27 GM, which is in agreement with previously reported values for fluorescein that range from 30 to 50 GM (31, 32, 36). HEK cells loaded with

RVF5 and imaged using two-photon laser scanning microscopy ($\lambda_{ex} = 820$ nm) displayed clear membrane-localized fluorescence (Fig. 3*A*) that showed a quadratic dependence on illumination intensity, consistent with pure two-photon absorbance (*SI Appendix*, Fig. S4). Under two-photon illumination, voltage sensitivity of RVF5 in HEK cells was ~24% (±7%, SEM for $n = 3$ separate experiments) ΔF/F per 100 mV, when considering pixels only at the cell membrane (Fig. 3 *C* and *D*). When a region of interest included pixels within the dim cytosol, the calculated voltage sensitivity was lower, at 17% ΔF/F per 100 mV (*SI Appendix*, Fig. S5). These results establish that RVF5, a molecular wire-based voltage indicator, can sense voltage under two-photon illumination.

Use of RVF5 in Neurons. With enhanced photostability and voltage sensitivity on par with previous generations of VF dyes, RVF5 should be well-suited to observing membrane voltage changes in neurons. Cultured rat hippocampal neurons bathed with RVF5 (200 nM) displayed clear membrane fluorescence when examined using one-photon, wide-field fluorescence microscopy (Fig. 4*A*). Field stimulation of neurons loaded with RVF5 resulted in optically recorded transients displaying ~11% ΔF/F per spike (±1%, $n = 10$ AP each from $n = 3$ neurons) with a signal-to-noise ratio of 10:1 (±1) (Fig. 4*B*). The improved photostability of RVF5 relative to VF2.1.Cl enabled longer recording from neurons and therefore imaging of spontaneous activity. Optical recording of rat hippocampal neurons stained with RVF5 (Fig. 4*C*) for 40-s periods revealed sparse spiking events, which could be collected from multiple cells simultaneously (Fig. 4*D*). Rat hippocampal neurons loaded with RVF5 were also subjected to whole-cell patch-clamp electrophysiology under current-clamp
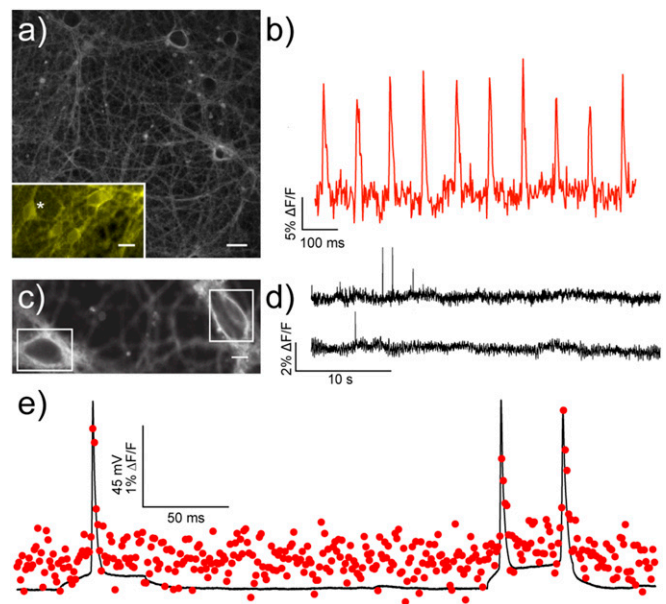

Fig. 4. One-photon characterization of RVF5 in neurons. (*A*) Dissociated rat hippocampal neurons stained with RVF5 and imaged under wide-field fluorescence microscopy conditions. (*Inset*) Image used for acquisition of data in *B*. (Scale bars, 20 μm.) (*B*) Trains of action potentials evoked by extracellular stimulation of neurons in *A* (*Inset*). Plot shows the average intensity from the neuron indicated by (*). (*C* and *D*) Imaging spontaneous activity in rat hippocampal neurons stained with RVF5. Traces on the right show the spontaneous activity in the boxed neurons in *C*. (Scale bar, 8 μm.) (*E*) Dual electrophysiological and optical recording of action potentials in cultured hippocampal neurons. Action potentials were evoked under current clamp mode and recorded electrophysiologically (black trace, 50-kHz sampling rate) and optically (red dots, 1-kHz sampling rate).

mode to evoke action potentials. Dual optical (red circles) and electrophysiological recording (black line) establish that RVF5 exactly follows the electrophysiological recording (Fig. 4E). Comparison of action potential parameters recorded electrophysiologically in cultured mouse hippocampal neurons with and without RVF5 shows no significant difference in action potential duration, rise, or decay time (*SI Appendix*, Fig. S6), suggesting that RVF5 does not perturb cellular physiology.

RVF5 To Measure Disease Phenotypes. The ability to monitor neural activity with cellular resolution for extended recording periods is important for deciphering the role individual neurons play in the context of larger networks. This resolution would be especially useful for elucidating disease mechanisms in models of human disorders characterized by altered neuronal activity, such as epilepsy. For example, the human neurodevelopmental disorder TSC is characterized by epilepsy, autism spectrum disorder, and cognitive disability (37) and results from loss of function mutations in the *TSC1* or *TSC2* genes. The protein products of these genes form a complex that negatively regulates mTOR signaling, however the mechanisms by which changes in mTOR signaling lead to deregulated neural activity are not well understood (38–40). In mice, loss of *Tsc1* leads to imbalances in synaptic excitation/inhibition, increased overall network activity, and seizures, which are a hallmark of this disorder (41). Previously, MEA recordings from control and Tsc1 knockout (KO) neurons in hippocampal cultures showed a clear difference in the activity of Tsc1 KO neurons, with Tsc1 KO cultures displaying higher rates of activity and burst firing (groups of action potentials) relative to controls (41). However, MEA recordings cannot provide the spatial information required to match bursting patterns to individual cells, precluding subtype-specific characterization or further analysis of how single cells may affect the properties of the entire network. Additionally, MEAs cannot give a concrete measure of the number of silent cells within a particular network, which may play an important role in determining overall network properties.

To address these open questions, dissociated hippocampal neuronal cultures were prepared from mice with conditional alleles of *Tsc1* (*Tsc1fl/fl*) (41, 42), cultured in vitro, and treated with a lentivirus encoding mCherry-tagged Cre recombinase to delete the *Tsc1* gene. This strategy provided paired sets of neurons from the same mouse that differed in their expression of Tsc1 (WT or KO). Following infection, neurons showed nuclear-localized mCherry signal, identifying Tsc1 KO neurons (Fig. 5B). After 14 d in vitro (DIV), neurons were incubated with RVF5 (Fig. 5A) and imaged for 40-s intervals to determine the spontaneous firing rate of the paired WT and Tsc1 KO samples. Optical records of spontaneous activity were acquired for over 50 individual neurons for both WT (n = 72; Fig. 5C, black trace) and Tsc1 KO (n = 54; Fig. 5C, red trace). We developed a custom script to enable rapid processing and extraction of spike timings from the acquired data (*SI Appendix*). Briefly, the fluorescence intensity vs. time for each neuron was plotted, and the SD for a nonspiking period of the recording was determined. Any time point 3 SDs above the mean baseline was considered a spike. Tsc1 KO neurons show a significantly higher average firing rate (9.2 ± 1.6 Hz, SEM) than their matched WT counterparts (4.3 ± 0.8 Hz, P < 0.01, Student's t test) (Fig. 5 D and E and *SI Appendix*, Fig. S7A), not including silent cells (see below). This result is consistent with previously reported observations from MEA data (~13 and 5 Hz per electrode for WT and KO cultures, respectively) (41). Voltage imaging with RVF5 represents an improvement in cellular resolution over MEA recording, because spikes are sorted per neuron, as opposed to per electrode. Control experiments indicate that treatment with tetrodotoxin (1 μM), a
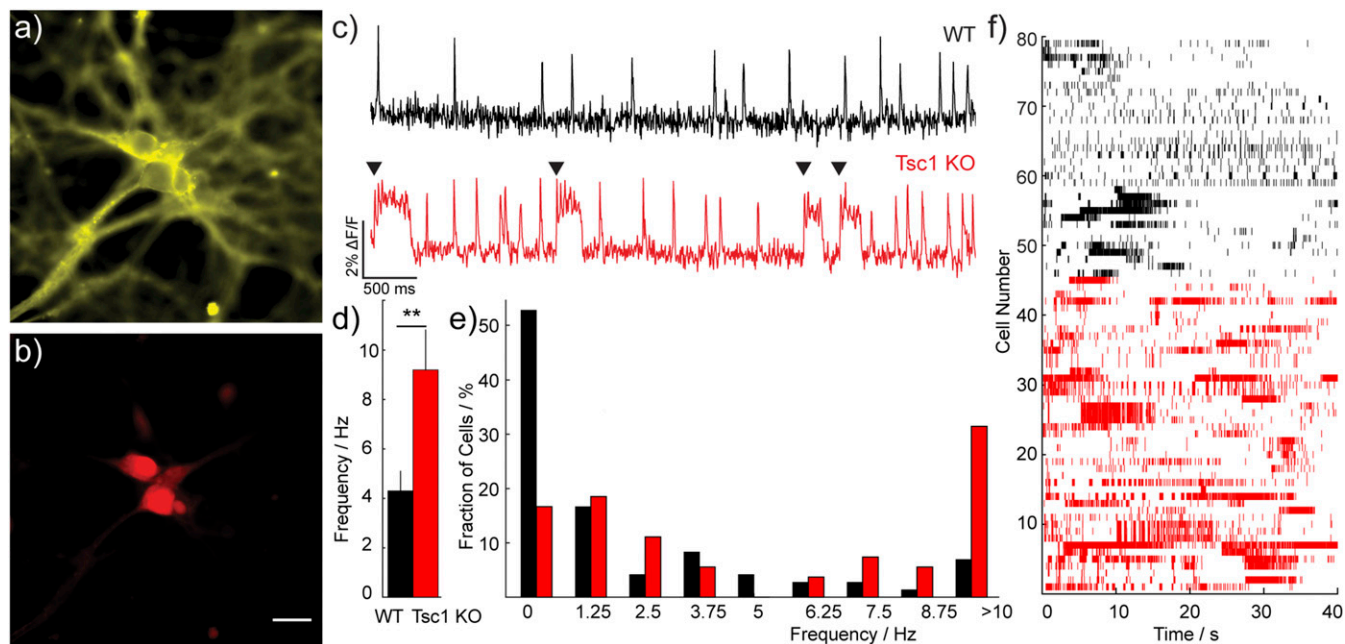
Fig. 5. Assessing differences in spontaneous activity in WT and Tsc1 KO neurons with RVF5. Wide-field fluorescence image of RVF5 staining (A) in DIV 14 cultured *Tsc1fl/fl* mouse hippocampal neurons infected with a virus encoding mCherry-Cre to knock out the *Tsc1* gene (Tsc1 KO). (B) mCherry labels Cre-expressing Tsc1 KO neurons. (C) Representative optical recordings of spontaneous activity in pairs of wild-type (WT, upper, black trace) and Tsc1 KO cultures (Tsc1 KO, lower, red trace). Arrowheads (▼) indicate periods of "burst" firing in the Tsc1 KO neuron. (D) Average spiking frequency, in hertz, for active WT and Tsc1 KO neurons. Error bars are SEM for n = 72 and 54 neurons for WT and Tsc1 KO, respectively. ** indicates P < 0.01, Student's two-tailed t test. (E) Histogram displaying fraction of total cells vs. firing frequency during a recording session for both WT (black) and Tsc1 KO (red) neurons. (F) Raster plot depicting spiking activity for all spontaneously active neurons. Each line represents a single spike detected in a given cell during the 40-s recording window for both WT (black) and Tsc1 KO (red) neurons. Each horizontal row depicts the spiking activity of a single neuron over time. (Scale bar is 20 μm for A and B.)

sodium channel blocker, completely abolishes spontaneous spiking activity in neurons (*SI Appendix*, Fig. S8A) while not affecting voltage sensitivity in HEK cells (*SI Appendix*, Fig. S8 *C* and *B*), establishing that these spikes reflect action potentials.

A raster plot displaying all spikes from across all imaging experiments clearly shows the higher density of action potentials in neurons lacking Tsc1 (Fig. 5 *E* and *F*). Interestingly, over half (38 of 72, 53%) of WT neurons were silent (Fig. 5E, See *SI Appendix*, Fig. S9 *A* and *B*), while only 9 of 54 (17%) Tsc1 KO neurons were silent (Fig. 5E and *SI Appendix*, Fig. S9 *C* and *D*) across all trials. The proportion of neurons firing at intermediate rates (>0–4 Hz) was similar across both WT and Tsc 1 KO neurons at 30% and 37%, respectively (n = 72 for WT, 54 for KO, Fig. 5e and *SI Appendix*, Fig. S7B), whereas the proportion of highly active (>4 Hz) neurons increases in the Tsc1 KO condition (17% WT vs. 46% KO; *SI Appendix*, Fig. S7B). These results show that loss of Tsc1 increases not only the firing rate, but the proportion of cells within the network that are active. Voltage imaging with RVF5 offers an expedient method for assessing global network properties (such as spike rate) while maintaining cellular specificity and resolution.

RVF5 and Two-Photon Imaging in Tissues. To lay the groundwork for further exploration of the roles of Tsc1 in neuronal excitability in the context of intact circuits, we assessed the ability of RVF5 to monitor neuronal activity ex vivo in mouse brain slices. Bath application of 10 μM RVF5 to brain slices acutely prepared from mice injected unilaterally with the mCherry-Cre virus (Tsc1 KO) or a sham (WT) into hippocampal area CA1 results in clearly defined membrane staining (Fig. 6 *C* and *D* and *SI Appendix*, Fig. S10 *A* and *B*). The fluorescence staining closely matched the cellular anatomy of the local brain region. For example, in cortical slices stained with RVF5, cell bodies of neurons appeared as dark cavities against a bright background of fluorescent membrane (*SI Appendix*, Fig. S10B). In the hippocampus, the highly stratified neuroanatomy (Fig. 6 *A*–*C*) is easily visualized at ~50 μm below the surface, in particular in the CA1 region where the cell bodies appear as a single dark band, highlighted by RVF5 staining of the membranes separating distinct cell bodies (Fig. 6 *C* and *D* and *SI Appendix*, Fig. S10A). Above and below the cell body layer, the basal and apical dendrites appear as a homogeneous stain, indicating the nonspecific uptake of RVF5 into cellular membranes. The expression of nuclear-localized mCherry confirmed successful Cre expression in the CA1 hippocampal subfield (Fig. 6 *D* and *E*).

We made optical recordings under two-photon (2P) illumination for 20–40 s in the CA1 region of the hippocampus. In single-trial, single-pixel (6.6 μm^2) optical recordings in oxygenated ACSF, both WT and Tsc1 KO slices show minimal activity, as measured by fractional changes in RVF5 fluorescence (Fig. 6F and *SI Appendix*, Fig. S10). Addition of the excitatory neurotransmitter glutamate to the slices results in robust induction of spiking behavior in both the WT and Tsc1 KO slices due to strong activation of excitatory synapses (Fig. 6G and *SI Appendix*, Fig. S10), similar to what we observe in single-unit, whole-cell electrophysiological recordings in neurons from CA1 in hippocampal slices (*SI Appendix*, Fig. S11). Our imaging field of view, comprising ~425 × 52 μm, allows us to sample a large number of neurons within the CA1; however, the fast sampling rates required for voltage imaging (>200 Hz) required trade-offs in spatial resolution, making distinguishing single cells in the functional imaging data difficult. Cellular resolution is further complicated by the fact that RVF5 efficiently stains all membranes, obscuring the assignment of fluorescence signals to single cells. Despite this challenge, at our current resolution and speed, we can clearly observe distinct firing patterns even in adjacent pixels (*SI Appendix*, Fig. S10 *C*–*F*, Tsc1 KO traces), providing sub-10-μm resolution of neuronal activity at a rate of ~200 Hz. These results show the utility of RVF5 for profiling neuronal activity in brain tissues.

Conclusions and Outlook

In summary, we present the design, synthesis, and applications of RVF5, a molecular wire-based molecular wire voltage-sensitive dye that features a rhodol scaffold for improved photostability and 2P absorption. Under both 1P and 2P illumination, RVF5 shows good voltage sensitivity and improved photostability compared with first-generation VF dyes. Additionally, we demonstrate that molecular wire-based voltage sensors efficiently report membrane potential dynamics under two photon illumination.

Incorporation of a rhodol fluorophore into a molecular wire voltage-sensing platform dramatically improves the 2P performance of VF-type dyes. Under 2P illumination, RVF5 displays an approximately fourfold increase in 2P absorption cross-section relative to VF2.1.Cl, while maintaining high voltage sensitivity. Previous studies on the 2P voltage sensitivity of both small-molecule (43) and genetically encoded voltage indicators (21)
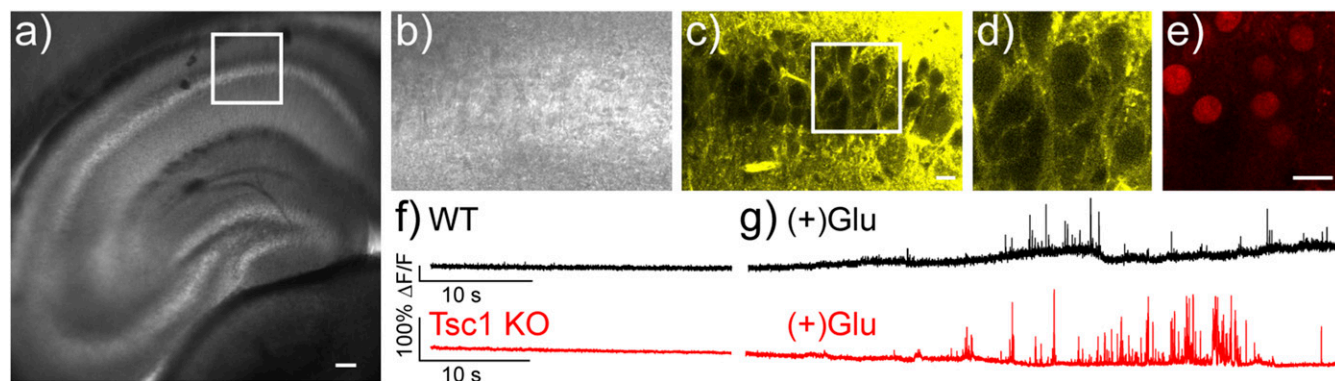
Fig. 6. Two-photon voltage imaging in mouse brain slices. Transmitted light images of mouse hippocampal brain slice stained with 10 μM RVF5 in oxygenated ACSF show (*A*) the entire hippocampus and (*B*) a zoomed region of CA1. (*C*) Fluorescence signals from RVF5 (10 μM, oxygenated ACSF) from the same region in *B* show membrane-localized staining. (*D* and *E*) A zoomed-in region from *C* shows RVF5 fluorescence primarily in cellular membranes and excluded from the cytosol and (*E*) nuclear-localized mCherry-Cre indicating Tsc1 KO neurons. Functional imaging was performed by creating an 8 × 64-pixel region over an area of CA1 and imaging at ~200 Hz for 20–40 s, first in the absence of glutamate (*F*) and then following addition of glutamate to the perfusate [panel *G*, (+)Glu]. Responses were recorded from neurons in the sham injected (control, WT, black traces) and mCherry-Cre injected (Tsc1 KO, red traces) hemispheres. (Scale bars, 100 μm for *A* and 20 μm for *B*–*E*.) Fluorescence traces are single-trial ΔF/F values from single pixels and are uncorrected for photobleaching.

reveal that the voltage sensing behavior under 2P illumination is not always identical to properties under 1P illumination. This study provides evidence that the voltage sensitivity of RVF5 is largely similar under both 1P and 2P conditions ($28 \pm 1\%$ vs. $24 \pm 7\%$ $\Delta F/F$ per 100 mV, respectively).

Small-molecule voltage-sensitive dyes have been previously used under 2P illumination conditions (44). However, styryl dyes used in these studies typically have σ_{TPA} values in the range of 5–10 GM, and maximal voltage sensitivity is only achieved by excitation at the very far edge of the 1P excitation spectrum (43), necessitating the loss of many incident photons and increasing phototoxicity. In contrast, PeT-based probes, like RVF5, can be excited at or near their excitation peaks, maximizing the useful number of photons delivered to tissue. On-peak excitation mitigates phototoxicity and is critically important for voltage imaging, because the high optical sampling rates required to image fast-spiking events restrict photon collection time, severely hampering sensitivity.

The improved photostability of RVF5 enables long-term recording of network activity with cellular resolution in a mouse model of the epilepsy disorder TSC. Our voltage imaging results are consistent with MEA recordings and further reveal that Tsc1 KO alters network properties by increasing the proportion of highly active cells relative to WT neurons. Simultaneously, voltage imaging with RVF5 provides a means to correlate recorded activity to individual cells for post hoc analysis (e.g., for cell-type confirmation). Finally, the increased 2P absorption cross-section of RVF5 enables deep-tissue imaging of voltage dynamics in hippocampal brain slices.

Methods

Detailed supporting information, including cell and tissue culture conditions, synthetic schemes and characterization, imaging parameters, and supporting figures and data are available online. Requests for reagents should be addressed to E.W.M. at evanwmiller@berkeley.edu.

1. Spira ME, Hai A (2013) Multi-electrode array technologies for neuroscience and cardiology. *Nat Nanotechnol* 8(2):83–94.
2. Peterka DS, Takahashi H, Yuste R (2011) Imaging voltage in neurons. *Neuron* 69(1): 9–21.
3. Miller EW (2016) Small molecule fluorescent voltage indicators for studying membrane potential. *Curr Opin Chem Biol* 33:74–80.
4. Davila HV, Salzberg BM, Cohen LB, Waggoner AS (1973) A large change in axon fluorescence that provides a promising method for measuring membrane potential. *Nat New Biol* 241(109):159–160.
5. Braubach O, Cohen LB, Choi Y (2015) Historical overview and general methods of membrane potential imaging. *Membrane Potential Imaging in the Nervous System and Heart, Advances in Experimental Medicine and Biology*, eds Canepari M, Zecevic D, Bernus O, Vol 859, pp 3–26.
6. Yan P, et al. (2012) Palette of fluorinated voltage-sensitive hemicyanine dyes. *Proc Natl Acad Sci USA* 109(50):20443–20448.
7. Kuhn B, Fromherz P (2003) Anellated hemicyanine dyes in a neuron membrane: Molecular Stark effect and optical voltage recording. *J Phys Chem B* 107(31): 7903–7913.
8. Hubener G, Lambacher A, Fromherz P (2003) Anellated hemicyanine dyes with large symmetrical solvatochromism of absorption and fluorescence. *J Phys Chem B* 107(31): 7896–7902.
9. Treger JS, Priest MF, Iezzi R, Bezanilla F (2014) Real-time imaging of electrical signals with an infrared FDA-approved dye. *Biophys J* 107(6):L09–L12.
10. Fink AE, Bender KJ, Trussell LO, Otis TS, DiGregorio DA (2012) Two-photon compatibility and single-voxel, single-trial detection of subthreshold neuronal activity by a two-component optical voltage sensor. *PLoS One* 7(8):e41434.
11. González JE, Tsien RY (1995) Voltage sensing by fluorescence resonance energy transfer in single cells. *Biophys J* 69(4):1272–1280.
12. Chanda B, et al. (2005) A hybrid approach to measuring electrical activity in genetically specified neurons. *Nat Neurosci* 8(11):1619–1626.
13. Ghitani N, Bayguinov PO, Ma Y, Jackson MB (2015) Single-trial imaging of spikes and synaptic potentials in single neurons in brain slices with genetically encoded hybrid voltage sensor. *J Neurophysiol* 113(4):1249–1259.
14. Reeve JE, et al. (2013) Porphyrins for probing electrical potential across lipid bilayer membranes by second harmonic generation. *Angew Chem Int Ed Engl* 52(34): 9044–9048.
15. Park K, Deutsch Z, Li JJ, Oron D, Weiss S (2012) Single molecule quantum-confined Stark effect measurements of semiconductor nanoparticles at room temperature. *ACS Nano* 6(11):10013–10023.
16. Marshall JD, Schnitzer MJ (2013) Optical strategies for sensing neuronal voltage using quantum dots and other semiconductor nanocrystals. *ACS Nano* 7(5):4601–4609.
17. Gong Y, et al. (2015) High-speed recording of neural spikes in awake mice and flies with a fluorescent voltage sensor. *Science* 350(6266):1361–1366.
18. St-Pierre F, et al. (2014) High-fidelity optical reporting of neuronal electrical activity with an ultrafast fluorescent voltage sensor. *Nat Neurosci* 17(6):884–889.
19. Hochbaum DR, et al. (2014) All-optical electrophysiology in mammalian neurons using engineered microbial rhodopsins. *Nat Methods* 11(8):825–833.
20. Jin L, et al. (2012) Single action potentials and subthreshold electrical events imaged in neurons with a fluorescent protein voltage probe. *Neuron* 75(5):779–785.
21. Brinks D, Klein AJ, Cohen AE (2015) Two-photon lifetime imaging of voltage indicating proteins as a probe of absolute membrane voltage. *Biophys J* 109(5):914–921.
22. Li LS (2007) Fluorescence probes for membrane potentials based on mesoscopic electron transfer. *Nano Lett* 7(10):2981–2986.
23. Miller EW, et al. (2012) Optically monitoring voltage in neurons by photo-induced electron transfer through molecular wires. *Proc Natl Acad Sci USA* 109(6):2114–2119.
24. Woodford CR, et al. (2015) Improved PeT molecules for optically sensing voltage in neurons. *J Am Chem Soc* 137(5):1817–1824.
25. Lavis LD, Raines RT (2008) Bright ideas for chemical biology. *ACS Chem Biol* 3(3): 142–155.
26. Huang YL, Walker AS, Miller EW (2015) A photostable silicon rhodamine platform for optical voltage sensing. *J Am Chem Soc* 137(33):10767–10776.
27. Kim HM, Cho BR (2015) Small-molecule two-photon probes for bioimaging applications. *Chem Rev* 115(11):5014–5055.
28. Dodani SC, et al. (2014) Copper is an endogenous modulator of neural circuit spontaneous activity. *Proc Natl Acad Sci USA* 111(46):16280–16285.
29. Whitaker JE, et al. (1992) Fluorescent rhodol derivatives: Versatile, photostable labels and tracers. *Anal Biochem* 207(2):267–279.
30. Drobizhev M, Makarov NS, Tillo SE, Hughes TE, Rebane A (2011) Two-photon absorption properties of fluorescent proteins. *Nat Methods* 8(5):393–399.
31. Xu C, Zipfel W, Shear JB, Williams RM, Webb WW (1996) Multiphoton fluorescence excitation: New spectral windows for biological nonlinear microscopy. *Proc Natl Acad Sci USA* 93(20):10763–10768.
32. Makarov NS, Drobizhev M, Rebane A (2008) Two-photon absorption standards in the 550-1600 nm excitation wavelength range. *Opt Express* 16(6):4029–4047.
33. Albota MA, Xu C, Webb WW (1998) Two-photon fluorescence excitation cross sections of biomolecular probes from 690 to 960 nm. *Appl Opt* 37(31):7352–7356.
34. Poronik YM, Clermont G, Blanchard-Desce M, Gryko DT (2013) Nonlinear optical chemosensor for sodium ion based on rhodol chromophore. *J Org Chem* 78(23): 11721–11732.
35. Fisher JA, Salzberg BM, Yodh AG (2005) Near infrared two-photon excitation cross-sections of voltage-sensitive dyes. *J Neurosci Methods* 148(1):94–102.
36. Mütze J, et al. (2012) Excitation spectra and brightness optimization of two-photon excited probes. *Biophys J* 102(4):934–944.
37. Prather P, de Vries PJ (2004) Behavioral and cognitive aspects of tuberous sclerosis complex. *J Child Neurol* 19(9):666–674.
38. Fryer AE, et al. (1987) Evidence that the gene for tuberous sclerosis is on chromosome 9. *Lancet* 1(8534):659–661.
39. Cheadle JP, Reeve MP, Sampson JR, Kwiatkowski DJ (2000) Molecular genetic advances in tuberous sclerosis. *Hum Genet* 107(2):97–114.
40. Kwiatkowski DJ, Manning BD (2005) Tuberous sclerosis: A GAP at the crossroads of multiple signaling pathways. *Hum Mol Genet* 14 Spec No. 2:R251–R258.
41. Bateup HS, et al. (2013) Excitatory/inhibitory synaptic imbalance leads to hippocampal hyperexcitability in mouse models of tuberous sclerosis. *Neuron* 78(3):510–522.
42. Kwiatkowski DJ, et al. (2002) A mouse model of TSC1 reveals sex-dependent lethality from liver hemangiomas, and up-regulation of p70S6 kinase activity in Tsc1 null cells. *Hum Mol Genet* 11(5):525–534.
43. Kuhn B, Fromherz P, Denk W (2004) High sensitivity of Stark-shift voltage-sensing dyes by one- or two-photon excitation near the red spectral edge. *Biophys J* 87(1): 631–639.
44. Fisher JAN, et al. (2008) Two-photon excitation of potentiometric probes enables optical recording of action potentials from mammalian nerve terminals in situ. *J Neurophysiol* 99(3):1545–1553.